Bulletin of the Seismological Society of America, Vol. 83, No. 2, pp. 330–346, April 1993

DETERMINATION OF EARTHQUAKE ENERGY RELEASE AND M_L USING TERRASCOPE

BY HIROO KANAMORI, JIM MORI, EGILL HAUKSSON, THOMAS H. HEATON, L. KATHERINE HUTTON, AND LUCILE M. JONES

ABSTRACT

We estimated the energy radiated by earthquakes in southern California using on-scale very broadband recordings from TERRAscope. The method we used involves time integration of the squared ground-motion velocity and empirical determination of the distance attenuation function and the station corrections. The time integral is typically taken over a duration of 2 min after the *P*-wave arrival. The attenuation curve for the energy integral we obtained is given by $q(r) = cr^{-n}\exp(-kr)(r^2 = \Delta^2 + h_{ref}^2)$ with $c = 0.49710$, $n = 1.0322$, $k = 0.0035$ km^{-1}, and $h_{ref} = 8$ km, where Δ is the epicentral distance. A similar method was used to determine M_L using TERRAscope data. The station corrections for M_L are determined such that the M_L values determined from TERRAscope agree with those from the traditional optical Wood-Anderson seismographs. For $1.5 < M_L < 6.0$, a linear relationship $\log E_S = 1.96\ M_L + 9.05$ (E_S in ergs) was obtained. However, for events with $M_L > 6.5$, M_L saturates. The ratio E_S / M_0 (M_0: seismic moment), a measure of the average stress drop, for six earthquakes, the 1989 Montebello earthquake ($M_L = 4.6$), the 1989 Pasadena earthquake ($M_L = 4.9$), the 1990 Upland earthquake ($M_L = 5.2$), the 1991 Sierra Madre earthquake ($M_L = 5.8$), the 1992 Joshua Tree earthquake ($M_L = 6.1$), and the 1992 Landers earthquake ($M_w = 7.3$), are about 10 times larger than those of the others that include the aftershocks of the 1987 Whittier Narrows earthquake, the Sierra Madre earthquake, the Joshua Tree earthquake, and the two earthquakes on the San Jacinto fault. The difference in the stress drop between the mainshock and their large aftershocks may be similar to that between earthquakes on a fault with long and short repeat times. The aftershocks, which occurred on the fault plane where the mainshock slippage occurred, had a very short time to heal, hence a low stress drop. The repeat time of the major earthquakes on the frontal fault systems in the Transverse Ranges in southern California is believed to be very long, a few thousand years. Hence, the events in the Transverse Ranges may have higher stress drops than those of the events occurring on faults with shorter repeat times, such as the San Andreas fault and the San Jacinto fault. The observation that very high stress-drop events occur in the Transverse Ranges and the Los Angeles Basin has important implications for the regional seismic potential. The occurrence of these high stress-drop events near the bottom of the seismogenic zone strongly suggests that these fault systems are capable of supporting high stress that will eventually be released in major seismic events. Characterization of earthquakes in terms of the E_S / M_0 ratio using broadband data will help delineate the spatial distribution of seismogenic stresses in the Los Angeles basin and the Transverse Ranges.

INTRODUCTION

The energy involved in an earthquake includes the strain energy change, W; the energy radiated in seismic wave, E_S; heat loss during faulting H; potential energy due to deformation, E_p; and energy for creation of fractures, E_c. Here,

E_S includes both kinetic and strain energy carried by seismic waves and is, on the average, twice the kinetic energy.

Since it is not possible to determine the absolute tectonic stress in the crust with a seismological method, W cannot be determined directly from seismic waves. Likewise, H and E_c cannot be determined directly. The only energy that can be determined from seismological data is E_S. Even though E_S represents only a part of the energy budget associated with an earthquake, it is still a very important physical quantity associated with it. In view of this, many studies have been made to estimate E_S from seismic radiation, for example Gutenberg and Richter (1942, 1956a, b), Bath (1966), Thatcher and Hanks (1973), Boatwright and Choy (1985), Vassiliou and Kanamori (1982), Bolt (1986), Kikuchi and Fukao (1988), and Houston (1990a, b).

Gutenberg and Richter (1956a) established an empirical relation, $\log E_S = aM + b$, between earthquake magnitude M and E_S where a and b are constants. The most widely used relation is the one between E_S and the surface-wave magnitude M_S: $\log E_S = 1.5\ M_S + 11.8$ (E_S in ergs). The energy E_S is estimated in two ways. In the first method, the ground motion velocity of radiated waves, either body or surface waves, is squared and integrated to estimate E_S. In this case, the major difficulties are obtaining complete coverage of the focal sphere and in the correction of the propagation effects, i.e., geometrical spreading, attenuation, waveguide effects, and scattering. If a large amount of data is available, one can estimate E_S with several empirical corrections and assumptions. The second method involves determination of the source function by inversion of seismograms. In this case, the propagation effects are removed through the process of inversion, but the solution is usually bandlimited. Nevertheless, with the advent of sophisticated inversion methods, this method has been used with considerable success (Kikuchi and Fukao, 1988). It is not easy to estimate the error in these determinations, but a factor of 5 error appears common.

With the development of a very broadband network, TERRAscope, in southern California, on-scale recordings of waveforms of local events at short distances have become available (Kanamori *et al.*, 1991). Because of the short distance, these records are not significantly contaminated by propagation effects and are thus suitable for accurate energy estimations. In this paper, we present a method for energy estimation from broadband records and apply it to many local events recorded with TERRAscope. Thatcher and Hanks (1973) made a similar attempt using the Wood-Anderson seismograms.

For many significant events, the seismic moment M_0 has been determined. Since M_0 represents the long-period end of the spectrum and E_S represents the integral of the spectrum over the entire frequency band, the ratio E_S/M_0 gives a measure of the average stress drop. We will show that this ratio varies significantly from place to place and between a mainshock and the associated aftershocks.

METHOD

For illustrative purposes, we use S waves and consider a station at a short distance from a point source. In this case, the observed wave is considered to be essentially the direct phase coming from the source, as is shown in Figure 1a. We consider a focal sphere at a distance r_0 from the source. Let v be the velocity of ground motion observed at a station. We estimate the particle-motion

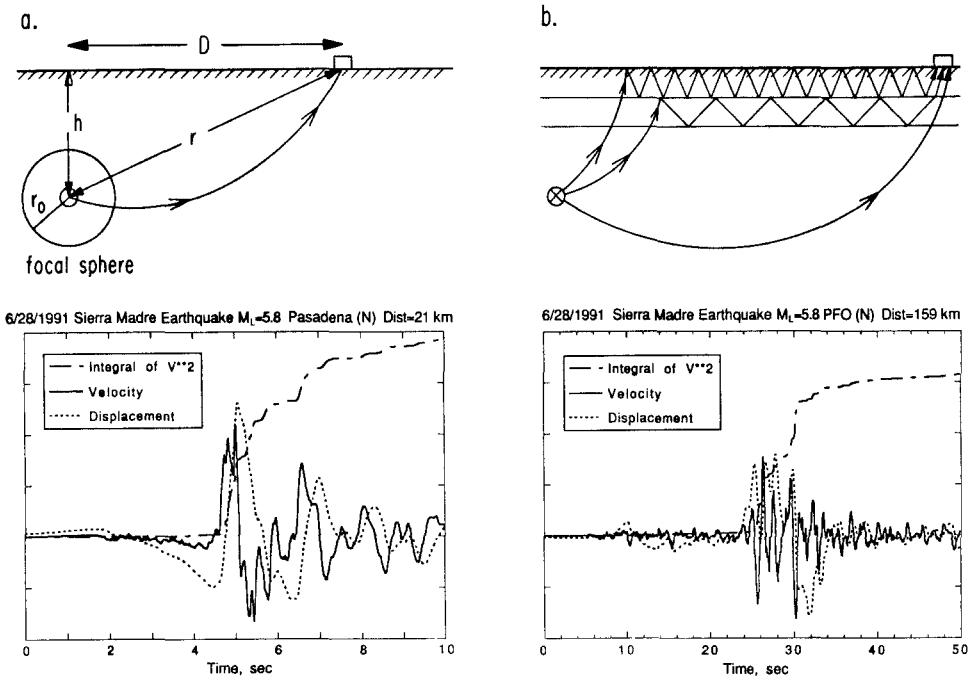

FIG. 1. (a) Schematic figure showing the ray geometry at a short distance and the focal sphere. A typical seismogram (displacement and velocity) and the integral of the squared velocity are shown below. (b) Schematic figure showing the ray geometry at a large distance. A typical seismogram (displacement and velocity) and the integral of the squared velocity are shown below.

velocity on the focal sphere, v_0, using the relation

$$v = v_0 C_f q(r)/q(r_0), \tag{1}$$

where C_f is the free-surface amplification factor, and r is the focal distance to the station (i.e., $r^2 = \Delta^2 + h^2$, Δ: epicentral distance, h: depth). The function $q(r)$ is the attenuation function. Implicit in this expression is that the effects of geometrical spreading, attenuation, reflection and refraction at weak structural boundaries, and scattering are all included in the attenuation function $q(r)$. This assumption is considered reasonable at short distances. For the first approximation, we use Richter's (1935) attenuation curve corrected by Jennings and Kanamori (1983), which can be closely approximated by

$$q(r) = cr^{-n}\exp(-kr), \qquad r^2 = \Delta^2 + h_{ref}^2, \tag{2}$$

with $c = 0.49710$, $n = 1.2178$, $k = 0.0053$ km^{-1}, and $h_{ref} = 8$ km. These constants are slightly different from those obtained by Hutton and Boore (1987), but the curve given by (2) is very similar to that given by them at distances shorter than 300 km. This attenuation function will be empirically modified later.

The S-wave energy radiating from the focal sphere can be expressed as

$$E_\beta = \rho_0 \beta_0 \int_{S_0}\int \sum v_0^2 \, dt \, dS, \tag{3}$$

where ρ_0 and β_0 are the density and S-wave velocity of the medium at the focal sphere (e.g., Haskell, 1964). The surface integral is taken over the focal sphere. The integration with time is to be taken over the S-wave train. Some ambiguity exists, however, regarding what the S-wave train is. We will discuss this problem later; here we assume that we can identify the S-wave train. The term Σv_0^2 represents the squared sum of the velocity of the vertical, radial, and transverse components.

Substituting (1) into (3), we obtain

$$E_\beta = C_f^{-2}[q(r_0)/q(r)]^2 \rho_0 \beta_0 \int_{S_0} \int \sum v^2 \, dt \, dS. \tag{4}$$

If the radiation pattern is ignored, v^2 does not depend on azimuth, and (4) can be reduced to

$$E_\beta = 4\pi r^2 C_f^{-2}[r_0 q(r_0)/rq(r)]^2 \rho_0 \beta_0 \int \sum v^2 \, dt. \tag{4'}$$

If the radiation pattern is to be included, we write $v = F(t)R$, where R is the radiation pattern as a function of azimuth and $F(t)$ is the common source time history. Then $\Sigma v^2 = F^2(t)\Sigma R^2$. We let subscript s to indicate the station being used and obtain

$$\sum v^2 = \sum v_s^2 \cdot \sum R^2 / \sum R_s^2. \tag{5}$$

Substitution of (5) into (4) leads to

$$E_\beta = C_f^{-2}[q(r_0)/q(r)]^2 \rho_0 \beta_0 \int \sum v_s^2 \, dt \int_{S_0} \sum R^2 \, dS / \sum R_s^2. \tag{6}$$

We define the average of the squared radiation-pattern factor by

$$\overline{R}^2 = \frac{1}{4\pi r_0^2} \int_{S_0} \sum R^2 \, dS. \tag{7}$$

From (6) and (7), we obtain

$$E_\beta = 4\pi r^2 C_f^{-2}[r_0 q(r_0)/rq(r)]^2 \rho_0 \beta_0 \int \sum v_s^2 \, dt \, \overline{R}^2 / \sum R_s^2. \tag{8}$$

For a double-couple source

$$\overline{R}^2 = \frac{1}{4\pi r_0^2} \int_{S_0} \sum R^2 \, dS = \frac{4}{15} \quad \text{and} \quad \frac{2}{5}$$

for P and S waves, respectively.

Equation (8) gives the estimate of energy from

$$\int \sum v_s^2 \, dt, \tag{9}$$

which can be directly computed from the seismograms recorded at the station.

In the present analysis, the energy attenuation curve is assumed to be independent of the event size. Since large earthquakes are more enriched in long-period energy than small earthquakes, the attenuation is expected to be less for large events. Since the distance range we used is usually less than 300 km, this effect is not important. For very small events with $M_L < 2.5$, however, the attenuation is very large and our energy estimate may be inaccurate.

In the method described above, a point source is assumed. However, the method needs to be modified for a large event with a finite fault. Since the energy radiation from the fault plane is most likely to be nonuniform, a rigorous calculation of energy would have to involve a detailed determination of the rupture process. For routine determination of energy, however, the simplest way would be to define a representative distance for a given fault-station geometry and use it in the point source equation (8). Since the energy is proportional to $1/r^2$ (r = distance), we may use the distance defined by

$$\bar{r} = \left(\frac{1}{S} \int \frac{1}{r^2} \, dS \right)^{-1/2},$$

where the integral is taken over the entire fault surface S.

Energy Determination

In practice, we assume that $\bar{R}^2/\Sigma R_s^2 = 1$, which is equivalent to using the average radiation pattern for all the stations. In this case (8) is identical to (4′). When the values from many stations are averaged, this approximation should be good. We also use the following numerical values: $\rho_0 = 2.5$ g/cm^3, $\beta_0 = 3$ km/sec, $r_0 = 8$ km ($= h_{ref}$). These values are appropriate for southern California events that are at mid-crustal depths. The free-surface amplification factor C_f is assumed to be 2 for the station Pasadena, which is located on basement rock. For other stations, the amplification effect caused by the near-receiver structure will be included in the station correction. Then, equation (8) yields

$$E_\beta = 23.6 \times 10^5 r^2 [r_0 q(r_0)/r q(r)]^2 \int \sum v_s^2 \, dt, \tag{10}$$

where r is in cm, $\int \Sigma v_s^2 \, dt$ is in cm^{2}sec^{-1}, and E_β is in ergs. The quantity in brackets in (10) can be computed from $q(r)$. Since the r dependence of $q(r)$ is different from r^{-1}, this quantity depends slightly on the choice of r_0, but the dependence is very small.

As mentioned earlier, it is not always obvious what the direct S-wave train is. When the rupture process is complex, the S wave is not an impulse but consists of several pulses. Also, even if the source is simple, the observed S wave may exhibit complex waveforms caused by the path effects, and it is not always possible to separate the source phase from the structure phase. For a large event, both phases arrive at the same time, making the separation almost

impossible. For a very large event with a fault length of 300 km, the rupture time may be as long as 2 min; hence the S-wave energy is expected to arrive over a duration of 2 min. In this study we use a long wave train, typically 2 min duration after the P-wave arrival. The advantage of taking the 2-min window is that we can almost certainly include all the energy coming from the source, even for a very large earthquake. The disadvantage is that the integration includes indirect S phases and surface waves at large distances. Since attenuation and geometrical spreading are different for S waves and surface waves, inclusion of surface waves causes errors in energy estimation. The P-wave contribution is negligible. For a double-couple source, the P-wave energy is only 4% of the S-wave energy (Haskell, 1964), which is much smaller than the error involved in the estimation of energy.

The method described above is initially developed for events at short distances where the direct S phase can be identified. At large distances, reflected and refracted S phases and surface waves contribute to the seismograms, as shown by Figure 1b, and many of the assumptions used above are no longer valid. However, we still apply the same method for events at distances up to 300 km. The error resulting from inclusion of the phases other than the direct S wave is minimized empirically by adjusting the attenuation function.

As mentioned above, Richter's attenuation curve $q(r)$ is used only as the first approximation. Richter's curve is for the maximum amplitude of the Wood-Anderson record and is not necessarily appropriate for the energy integral, which includes not only the S wave but also other phases. Hence, in the next step, we empirically determine the correction for $q(r)$ together with the station corrections.

Attenuation Function and Station Corrections

Let $e_{ij}^{\,0}$ be the energy of event j estimated from station i using the standard Richter attenuation curve, $q(r)$, without station correction. We computed $e_{ij}^{\,0}$ using equation (8) for 66 events recorded with TERRAscope during the period from January 1988 to December 1991 and for three events of the 23 April 1992, Joshua Tree sequence (foreshock, mainshock, and the largest aftershock). The locations of the earthquakes are shown in Figure 2 together with the TERRAscope stations. Then we computed the deviation of $\log e_{ij}^{\,0}$ from the average taken over the stations:

$$\Delta \log e_{ij}^{\,0} = \log e_{ij}^{\,0} - \frac{1}{N_s} \sum_{i=1}^{N_s} \log e_{ij}^{\,0}.$$

Figure 3a shows $\Delta \log e_{ij}^{\,0}$ thus determined as a function of distance. In addition to the large scatter, a clear distance dependence is seen. We now modify the attenuation curve and determine the station corrections to minimize the scatter. We follow the method described by Joyner and Boore (1981) and Bakun and Boore (1985).

Since the real attenuation curve is different from $q(r)$, the correct estimate of the energy e should be given by

$$e = e_{ij}^{\,0} \left(\frac{f(r_{ij})}{f(r_0)} \right) s_i, \tag{11}$$

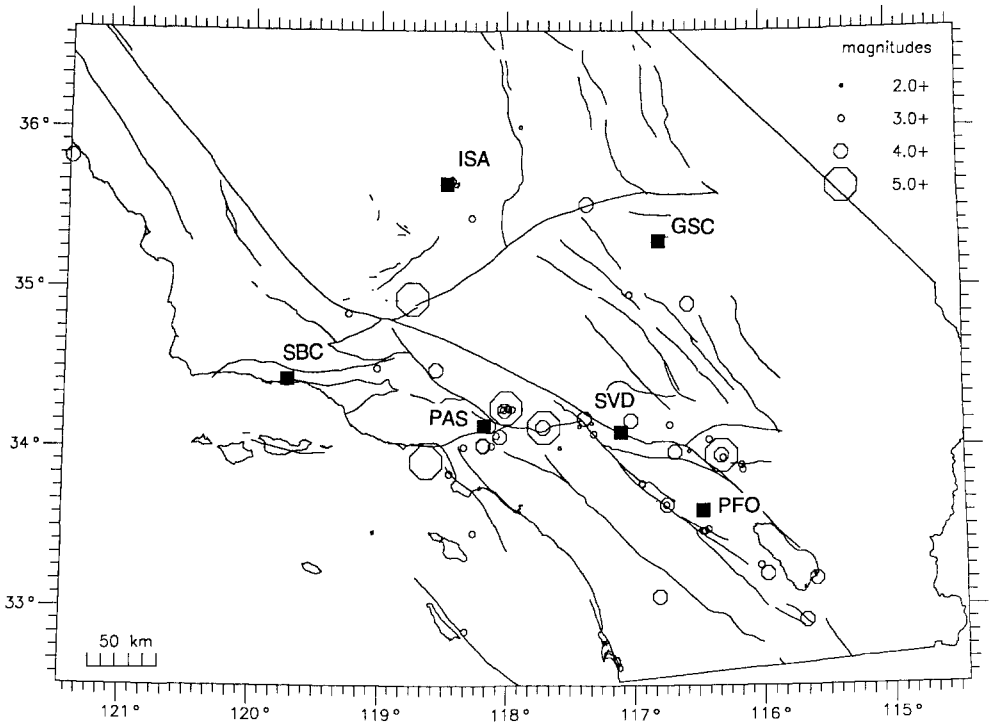

FIG. 2. TERRAscope stations (solid square) and the earthquakes used in this study (open symbols).

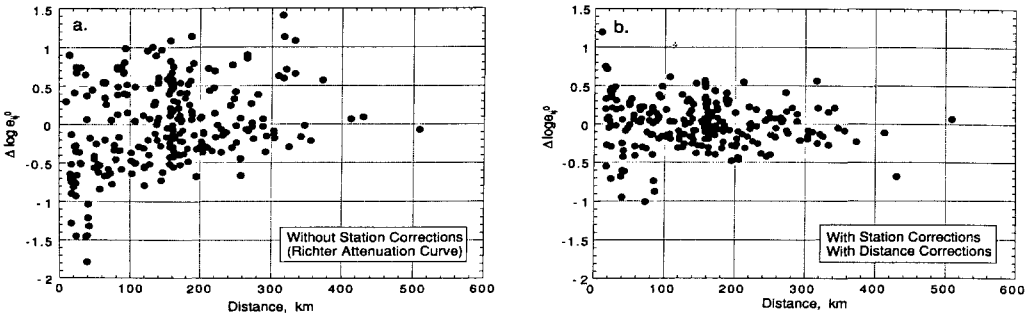

FIG. 3. (a) The deviation of the logarithm of energy, $\Delta \log e_{ij}^{\,0} = \log e_{ij}^{\,0} - (1/N_s)\Sigma_{i=1}^{N_s} \log e_{ij}^{\,0}$, as a function of distance. Richter's attenuation function is used, and no station corrections are applied. Note the large scatter due to the site effects and the distance bias. (b) The same as (a), but with the revised attenuation function and station corrections. Note the reduction in the scatter and absence of distance bias.

where s_i is the station correction, $f(r)$ is the correction factor for the attenuation curve, and r_0 is the radius of the focal sphere. To determine s_i and $f(r)$, we chose the station Pasadena as a reference station, for which the station correction is set equal to 1. Then

$$\left(\frac{e_{1j}^{\,0}}{e_{ij}^{\,0}}\right) = \left(\frac{f(r_{ij})}{f(r_{1j})}\right) s_i, \qquad i = 1, \ldots, N_s, \qquad j = 1, \ldots, N_e, \tag{12}$$

where the subscript $i = 1$ indicates PAS, and N_s and N_e are the number of stations and events, respectively. We assume the same form for $f(r)$ as $q(r)$, i.e., $f(r) = r^{-n}\exp(-kr)$, and perform regression on the logarithm of (12), i.e.,

$$\log\left(\frac{e_{1j}^{0}}{e_{ij}^{0}}\right) = -n\log\left(\frac{r_{ij}}{r_{1j}}\right) - k\log e\cdot(r_{ij} - r_{1j}) + \log s_i,$$
$$i = 1,\ldots,N_s, \qquad j = 1,\ldots,N_e. \quad (13)$$

Here, the unknown parameters to be determined are n, k, and s_i $(i = 2,\ldots,N_s)$. Once n, k, and s_i $(i = 2,\ldots,N_s)$ are determined, they are incorporated in (10) for the determination of energy from each station.

The corrected attenuation curve for the energy integral is

$$q(r) = cr^{-n}\exp(-kr), \qquad r^2 = \Delta^2 + h_{ref}^2, \quad (14)$$

with $c = 0.49710$, $n = 1.0322$, $k = 0.0035$ km^{-1}, and $h_{ref} = 8$ km. The station corrections are listed in Table 1. Since a large amount of data has been used to determine these constants, they are not expected to change significantly as more data are used.

Figure 3b shows $\Delta\log e_{ij}^{0}$ obtained with the new attenuation curve and the station corrections. The scatter is now significantly reduced and no distance dependence is seen. The average scatter in $\Delta\log e_{ij}^{0}$ is about ± 0.3, which means that the scatter in the energy estimates is about a factor of 4. Since we average, for each event, the energy values determined from all the stations, the energy estimate for each event is very stable.

M_L

A similar method was used to determine M_L using TERRAscope data. In this method, we first simulated Wood-Anderson seismograms from the broadband records, and determined M_L from each of the three components, using the standard method described by Richter (1935), and averaged them. Although there is some question about the magnification of the standard Wood-Anderson instrument (Uhrhammer and Collins, 1990), we used the standard magnification, 2800. Another difference from the original Richter's practice is that we used the vertical component as well as the horizontal components. In general, the M_L values computed from the vertical component are smaller than those from the horizontals. However, these differences are not important because they are absorbed in the station corrections, as explained below.

TABLE 1
STATION CORRECTIONS

	s_i	ΔM_L
PAS	1.00	0.13
GSC	0.383	−0.05
PFO	1.22	0.23
SBC	0.146	−0.16
ISA	1.15	0.22
SVD	0.105	−0.19

In this calculation, an attenuation curve in the form

$$q(r) = cr^{-n}\exp(-kr), \qquad r^2 = \Delta^2 + h_{ref}{}^2,$$

with $c = 0.49710$, $n = 1.2178$, $k = 0.0053$ km^{-1}, and $h_{ref} = 8$ km, which is fitted to the original Richter's curve, is used. For a short distance range, the correction for the attenuation curve suggested by Jennings and Kanamori (1983) is incorporated. Figure 4a shows

$$\Delta M_L = M_L - \frac{1}{N_s}\sum_{station} M_L,$$

where M_L is the uncorrected local magnitude determined from each station. The summation is taken over all the stations. Although the scatter is fairly large, no obvious distance dependence is seen.

In order to determine the station corrections, a method almost identical to that described for the energy is used. Initially, the station correction for Pasadena is set equal to 0 and is later adjusted so that the M_L values determined from the Pasadena TERRAscope station agree with those determined from the Southern California Seismic Network (SCSN) stations using the photographic Wood-Anderson seismograms and the traditional procedure. This adjustment ensures that there will be no systematic difference between M_L determined with TERRAscope and SCSN. The station corrections thus determined are shown in Table 1. The ΔM_L values computed with the station corrections are shown in Figure 4b. No correction for the attenuation function was necessary.

E_S VERSUS M_L

Figure 5 shows the relationship between the corrected log E_s and M_L determined for the events shown in Figure 2 and for the 1992 Landers earthquake. Over the range $1.5 < M_L < 6.0$, a linear relationship

$$\log E_S = 1.96M_L + 9.05 \quad (E_S \text{ in ergs}) \tag{15}$$

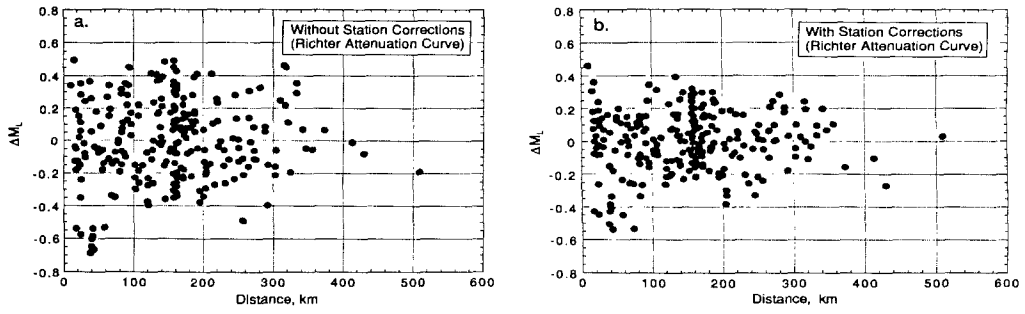

FIG. 4. (a) The deviation of M_L, $\Delta M_L = M_L - (1/N_s)\Sigma_{station} M_L$, determined from TERRAscope stations as a function of distance. Richter's attenuation function is used, and no station corrections are applied. Note the large scatter due to the site effects. (b) The same as (a), but with the station corrections.

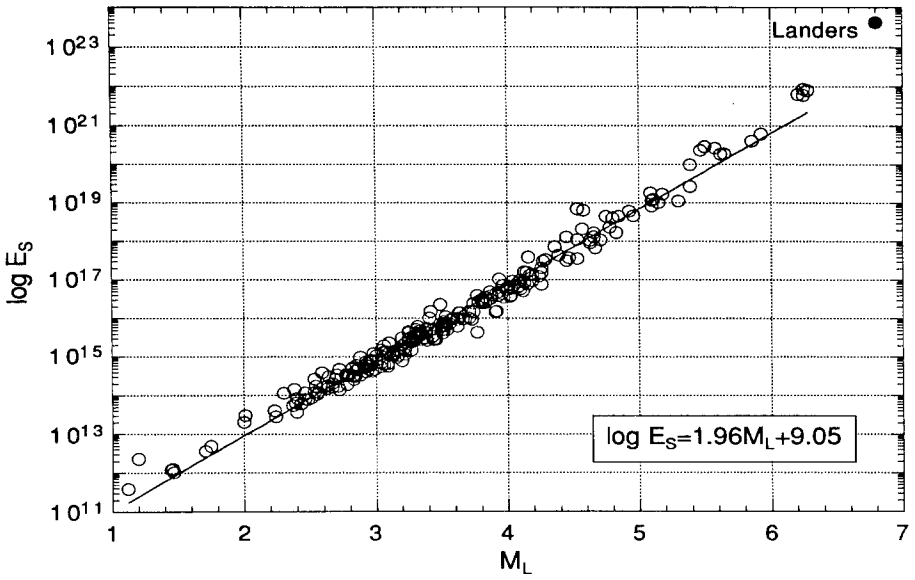

FIG. 5. The relation between Log E_S and M_L.

holds. This relation is in good agreement with the relation $\log E_S = 2.10M_L + 9.11$ obtained from a completely independent data set of 66 events obtained from low-gain stations and strong-motion instruments of SCSN (Jim Mori, personal comm., 1991). The slope is almost 2, which agrees with the result of Thatcher and Hanks (1973). This result indicates that the M_L scale gives a surprisingly good estimate of energy for events with $M_L \leqq 6.5$ despite its very simple definition.

For the events with $M_L \leqq 6.5$, M_L does not saturate with increasing E_S. However, as E_S increases further, M_L saturates, as indicated by the data point for the 1992 Landers earthquake. In this regard, $\log E_S$ is a more meaningful measure of the size of an earthquake. If we define a magnitude scale M_e using (15) (i.e., $M_e = (\log E_S - 9.05)/1.96$), it is consistent with M_L at small magnitudes and does not saturate at large magnitudes. For example, $M_e = 7.4$ for the 1992 Landers earthquake.

DISCUSSION

For the events listed in Table 2, the seismic moment, M_0, has been determined. The ratio E_S/M_0 is often used as a measure of the average stress drop (e.g., Vassiliou and Kanamori, 1982; Houston, 1990b). For a very simple model of faulting, such as the one suggested by Orowan (1960), in which the stress drops from σ_0 to σ_1 with a frictional stress σ_f, E_S is given by

$$E_S = W - H(\Delta\sigma/2\mu)M_0(1 + 2(\sigma_1 - \sigma_f)/\Delta\sigma). \tag{16}$$

Thus, if the final stress σ_1 is equal to the frictional stress σ_f, $E_S/M_0 = \Delta\sigma/2\mu$. However, if the fault process is more complex, and some energy is spent for creating new crack surfaces, $E_S/M_0 = e\,\Delta\sigma/2\mu$ where $e < 1$. Also, the final stress on the fault plane may not be equal to the frictional stress, so that the

TABLE 2

THE E_S / M_0 RATIO

Event	Date (m/d/y)	M_L^*	$M_L^\dagger$	M_0 (10^{23} dyne-cm)	E_S (10^{18} erg)	E_S/M_0 (10^{-5})	$\eta^\ddagger$
Whittier N. A	2/11/88	4.7	4.8	2.0[§]	0.8	0.40	2.1
Pasadena	12/3/88	4.9	4.6	2.4[¶]	20	8.3	0.36
Montebello	6/12/89	4.6	4.7	0.088[§]	1.1	13	2.0
Upland	2/28/90	5.2	5.5	25[#]	97**	3.9	
Sierra Madre	6/28/91	5.4	5.8	25[§]	280	11	
Sierra Madre A-1	6/28/91	4.3	4.5	0.40[§]	0.46	1.2	
Sierra Madre A-2	7/6/91	3.8	4.0	0.070[§]	0.033	0.47	
San Jacinto 1	5/20/91	3.7	3.6	0.030[§]	0.0058	0.19	
San Jacinto 2	5/20/91	3.5	3.3	0.016[§]	0.0024	0.15	
Joshua Tree F	4/23/92	4.6	4.7	0.31[††]	1.0	3.2	
Joshua Tree	4/23/92	6.1	6.1	190[††]	5100	27	
Joshua Tree A-1	4/23/92	4.1	3.9	0.10[††]	0.052	0.52	
Joshua Tree A-2	4/23/92	4.4	4.4	0.11[††]	0.41	3.7	
Joshua Tree A-3	4/26/92	4.2	4.4	0.49[††]	0.46	0.94	
Joshua Tree A-4	4/26/92	4.3	4.5	0.25[††]	0.33	1.3	
Joshua Tree A-5	4/27/92	4.2	4.3	0.26[††]	0.26	1.0	
Joshua Tree A-6	5/4/92	4.8	5.1	1.5[††]	7.3	4.9	
Joshua Tree A-7	5/12/92	4.4	4.5	0.39[††]	0.33	0.85	
Landers	6/28/92		6.8	11000[‡‡]	430000	39	

* From Southern California Catalog.

† From TERRAscope.

‡ η is the radiation pattern factor $\Sigma R_s^2/\bar{R}^2$. Since only one station (Pasadena) is used for the Whittier Narrows aftershock, Pasadena earthquake, and Montebello earthquake, the E_S values for these events estimated from the Pasadena record were divided by η.

§ Determined from waveform of close-in data using the method described in Kanamori (1990).

¶ Kanamori *et al.* (1990).

Dreger and Helmberger (1991).

** Single-station estimate.

†† Determined from surface-wave spectra (Hong-Kie Thio, written comm., 1992).

‡‡ Kanamori *et al.* (1992)

ratio E_S/M_0 may not necessarily give the estimate of the stress drop. Nevertheless, with this ambiguity in mind, we can use it as a useful parameter for comparing the dynamic characteristics of earthquakes.

Figure 6 shows the E_S/M_0 ratio for the earthquakes listed in Table 2. The stress drop values shown in Figure 6 are computed using $\Delta\sigma = 2\mu E_S/M_0$ with $\mu = 3 \times 10^{11}$ dynes/cm^2, but the absolute values should be interpreted with the uncertainty stated above. Figure 6 shows two important features. First, the earthquakes in the Transverse Ranges and the Los Angeles Basin (the 1989 Montebello earthquake ($M_L = 4.6$), the 1989 Pasadena earthquake ($M_L = 4.9$), the 1990 Upland earthquake ($M_L = 5.2$) and the 1991 Sierra Madre earthquake ($M_L = 5.8$), Fig. 7) and the Joshua Tree and Landers earthquakes have stress drops significantly higher than those of many large strike-slip earthquakes, computed by Kikuchi and Fukao (1988) from the E_S/M_0 ratios. The range of the E_S/M_0 ratios determined by Kikuchi and Fukao (1988) is indicated in Figure 6. Thatcher and Hanks (1973) earlier noted that the earthquakes in the Transverse Ranges have higher stress drops than those on the San Andreas, but the large scatter in the data set prevented them from making a definitive conclusion.

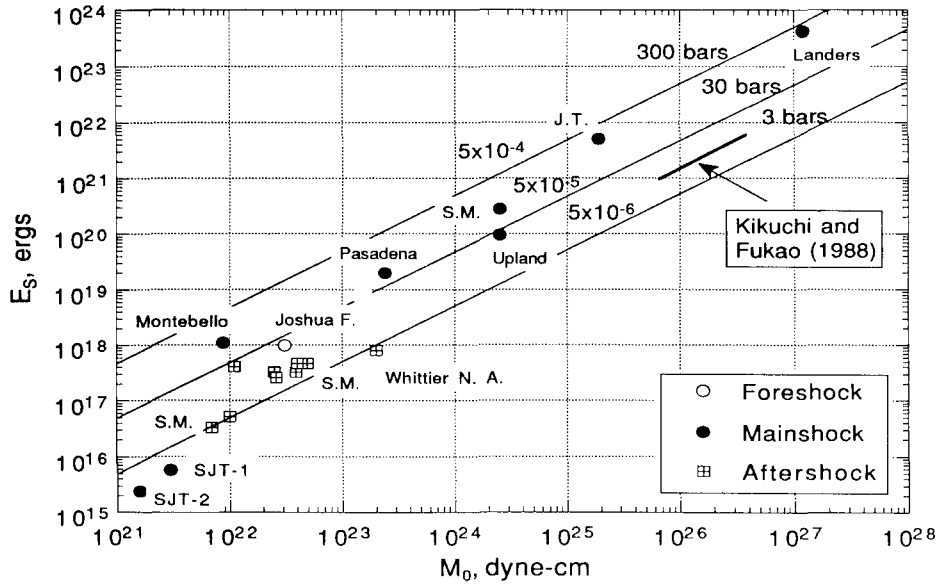

FIG. 6. The relation between seismic moment (M_0) and energy (E_S). J.T.: Joshua Tree, S.M.: Sierra Madre, SJT: San Jacinto Fault. The heavy solid line indicates the range of the E_S/M_0 ratios of large strike slip earthquakes determined by Kikuchi and Fukao (1988).

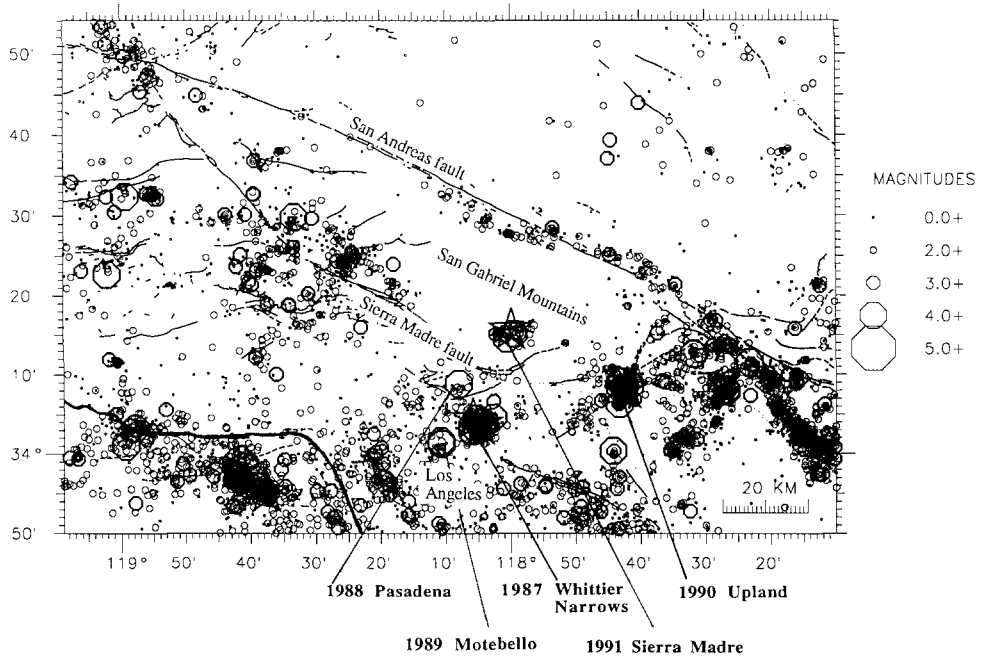

FIG. 7. Significant earthquakes in the Los Angeles basin and the Central Transverse Ranges. The asterisk indicates the events with $M \geq 5$.

This difference can be explained in terms of the difference in the repeat times. Kanamori and Allen (1986) presented evidence that earthquakes on faults with long repeat times radiate more energy per unit fault length than those with short repeat times. Houston (1990b) also found evidence for this. The implication is that the strength of a fault increases with the time during which the two sides of the fault have been locked. This may be viewed as a result of fault healing process. The repeat time of major earthquakes on the frontal fault systems in the Transverse Ranges is believed to be very long, a few thousand years (e.g., Crook *et al.*, 1987). Also, the overall slip rate of the faults in the eastern Mojave shear zone where the Joshua Tree and Landers earthquakes occurred is probably relatively low. Hence, the events in the Transverse Ranges, Joshua Tree, and Landers earthquakes are expected to have higher stress drops than those of the events occurring on faults with shorter repeat times, such as the San Andreas and the San Jacinto faults. Two earthquakes from the San Jacinto fault shown in Figure 6 do have smaller stress drops, but we have not yet observed significant events (i.e., $M_L > 5$) on either the San Andreas or the San Jacinto faults with TERRAscope, and a direct comparison has yet to be made.

The second important feature of Figure 6 is the difference in stress drops between the mainshock and aftershocks. The mainshock of the 1991 Sierra Madre earthquake (S.M., $M_L = 5.8$) and the Joshua Tree earthquake (J.T., 23 April 1992, $M_L = 6.1$) have E_S/M_0 ratios, hence stress drop, approximately 10 times larger than their aftershocks. The foreshock of the Joshua Tree earthquake has a stress drop higher than most of the aftershocks. This difference could also be explained in terms of the difference in the repeat time. Although we do not know exactly where aftershocks occur, some of them probably occur on the fault plane where the mainshock slippage occurred; these aftershocks have had a very short time to heal, hence a low stress drop. Some aftershocks that occur off the mainshock fault plane may have a higher stress drop. The variation of the stress drops among the aftershocks shown in Figure 6 may be reflecting this difference.

Figure 6 suggests that the E_S/M_0 ratio may vary around 5×10^{-5} by an order of magnitude for earthquakes in different tectonic provinces and structures, and this difference is important for understanding the difference in dynamic characteristics of earthquakes.

The result shown in Figure 6 is reflected in the pulse width of several close-in seismograms recorded at the Pasadena station. For earthquakes at short distances, the observed pulse width is approximately the same as width of the source time function, which is proportional to the source dimension. Figure 8 shows the pulse width of four earthquakes near Pasadena. The Pasadena earthquake (Fig. 8a) and the Whittier Narrows aftershock (Fig. 8b) have about the same magnitude, but the *SH* pulse width of the Pasadena earthquake is much narrower than that of the Whittier Narrows aftershock. The Sierra Madre earthquake (Fig. 8c) is about one magnitude unit larger than the Whittier Narrows aftershock, but both events have about the same *SH* pulse width. The Malibu earthquake (Fig. 8d) has a very broad *SH* pulse width, even though it is about the same size as the Pasadena earthquake and the Whittier Narrows earthquake. Figure 9 shows the relation between the pulse width and the seismic moment M_0 for the events listed in Table 3. The total duration of the triangular *SH* pulse is used here as the pulse width. A similar plot has been

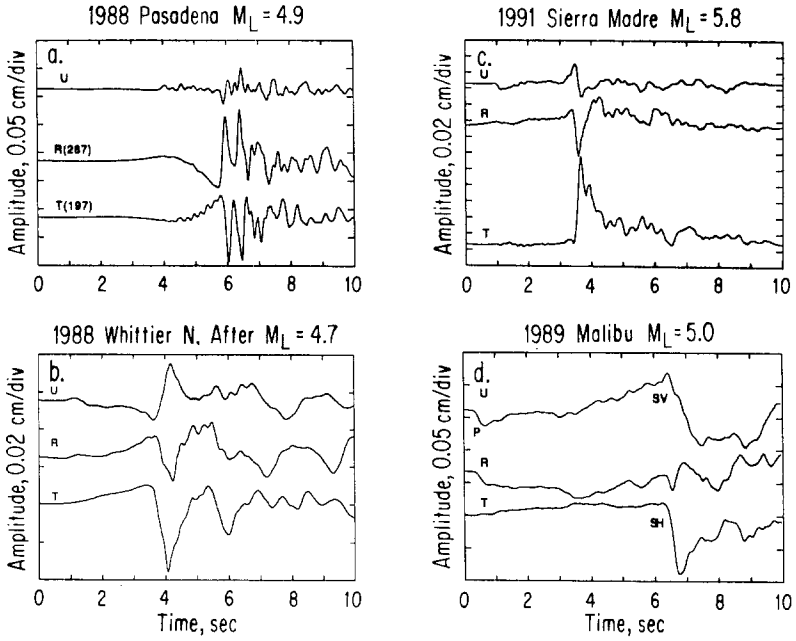

FIG. 8. Comparison of *SH* pulse width for four earthquakes near Pasadena.

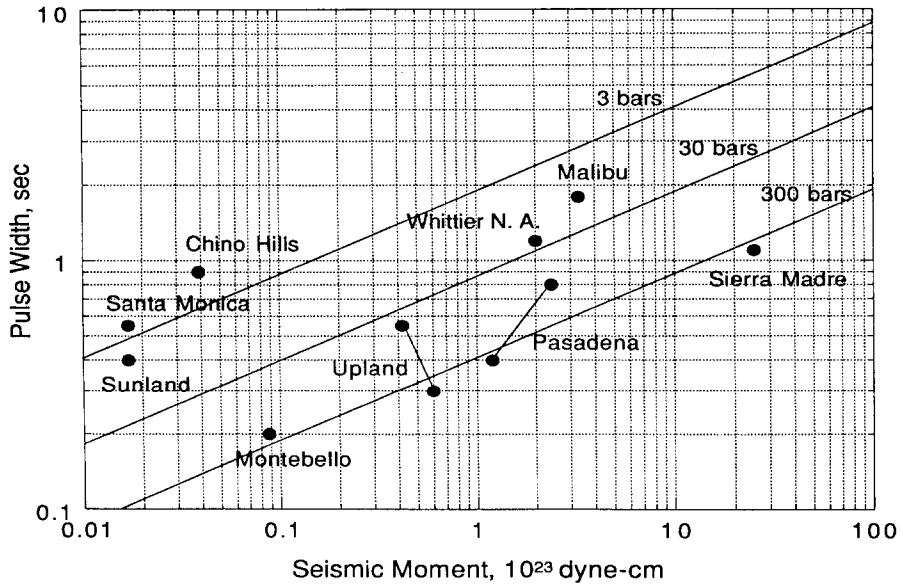

FIG. 9. Relation between the pulse width and M_0. The pulse width is determined from the total width. The straight lines show the trend for the constant stress drop. The stress-drop values shown on the curves are for a circular crack model. The absolute values depend on the rupture geometry. For the Pasadena and Upland earthquakes, the two solutions listed in Table 3 are shown and connected by solid lines.

TABLE 3

PULSE WIDTH AND SEISMIC MOMENT

Event	Date (m/d/y)	M_L^*	M_0 (10^{23} dyne-cm)	Pulse Width (sec)
Whittier N. A	2/11/88	4.7	2.0†	1.2
Pasadena	12/3/88	4.9	1.2‡	0.4‡
			2.4§	0.8§
Montebello	6/12/88	4.6	0.088†	0.2¶
Upland (aftershock)	6/26/88	4.7	0.42#	0.55#
			0.60**	0.3**
Sierra Madre	6/28/91	5.4	25†	1.1
Malibu	1/19/89	5.0	3.3†	1.8
Chino Hills	2/18/89	4.1	0.039†	0.9
Sunland	10/1/88	3.4	0.017†	0.55
Santa Monica	2/25/89	3.8	0.017†	0.40

* From Southern California Seismic Network Catalog.

† Determined from waveform of close-in data using the method described in Kanamori (1990).

‡ Kanamori *et al.* (1990), the first pulse of the *SH* wave.

§ Kanamori *et al.* (1990), the total *SH* wave.

¶ Measured from *P* wave (*SH* is nodal).

\# Mori and Hartzell (1990).

** Dreger and Helmberger (1990).

used by Cohn *et al.* (1982) and Somerville *et al.* (1987). The solid lines indicate the lines of constant stress drop. Although the absolute values of the stress drop depend on the rupture geometry, Figure 9 demonstrates that the 1989 Montebello, the 1989 Pasadena, and the 1991 Sierra Madre earthquakes have much larger stress drops than the other events, which is consistent with Figure 6.

The observation that very high stress-drop events occur in the Transverse Ranges and the Los Angeles Basin has important implications for the regional seismic potential. Although the mode of deformation (seismic versus aseismic) in the Los Angeles Basin and the Transverse Ranges is still a matter of debate, the occurrence of these high stress-drop events near the bottom of the seismogenic zone (Jones *et al.*, 1990, Hauksson and Jones, 1991; Hauksson, 1992) strongly suggests that these fault systems are capable of supporting high stress, which will eventually be released in major seismic events. Thus, characterization of earthquakes in terms of the E_S/M_0 ratio using broadband data will help delineate the spatial distribution of seismogenic stresses in southern California.

ACKNOWLEDGMENT

This research was partially supported by the U. S. Geological Survey Grant 14-08-0001-G1774 and grants from the L. K. Whittier Foundation and Arco Foundation. Contribution No. 5177, Division of Geological and Planetary Sciences, California Institute of Technology, Pasadena, California 91125.

REFERENCES

Bakun, W. H. and D. M. Boore (1985). The M_L scale in central California, *Bull. Seism. Soc. Am.* **74**, 1827–1843.

Bath, M. (1966). Earthquake energy and magnitude, in *Contributions in Geophysics: In Honor of Beno Gutenberg*, M. E. H. Benioff, B. F. Howell, Jr., and F. Press (Editors), Pergamon Press, New York.

Boatwright, J. and G. L. Choy (1985). Teleseismic estimates of the energy radiated by shallow earthquakes, in *U. S. Geol. Surv. Open-File Rept. 85-0290-A, Workshop XXVIII on the Borah Peak, Idaho earthquake*, R. S. Stein, R. C. Bucknam, and M. L. Jacobson (Editors), 409–448.

Bolt, B. A. (1986). Seismic energy release over a broad frequency band, *Pageoph* **124**, 919–930.

Boore, D. M. (1989). The Richter scale: its development and use for determining earthquake source parameters, *Tectonophysics* **166**, 1–14.

Cohn, S. N., T. L. Hong, and D. V. Helmberger (1982). The Oroville earthquakes: a study of source characteristics and site effects, *J. Geophys. Res.* **87**, 4585–4594.

Crook, R. J., C. R. Allen, B. Kamb, C. M. Payne, and R. J. Proctor (1987). Quaternary geology and seismic hazard of the Sierra Madre and associated faults, western San Gabriel Mountains, in *Recent Reverse Faulting in the Transverse Ranges, California, U. S. Geol. Surv. Profess. Pap. 1339*, D. M. Morton and R. F. Yerkes (Editors), 27–64.

Dreger, D. S. and D. V. Helmberger (1990). Broad-band modeling of local earthquakes, *Bull. Seism. Soc. Am.* **80**, 1162–1179.

Dreger, D. S. and D. V. Helmberger (1991). Complex faulting deduced from broadband modeling of the February 28, 1990 Upland earthquake (M_L = 5.2), *Bull. Seism. Soc. Am.* **81**, 1129–1144.

Gutenberg, B. and C. F. Richter (1942). Earthquake magnitude, intensity, energy, and acceleration, 1, *Bull. Seism. Soc. Am.* **32**, 163–191.

Gutenberg, B. and C. F. Richter (1956a). Earthquake magnitude, intensity, energy, and acceleration, *Bull. Seism. Soc. Am.* **46**, 105–145.

Gutenberg, B. and C. F. Richter (1956b). Magnitude and energy of earthquakes, *Ann. Geofis. Rome* **9**, 1–15.

Haskell, N. (1964). Total energy and energy spectral density of elastic wave radiation from propagating faults, *Bull. Seism. Soc. Am.* **56**, 1811–1842.

Hauksson, E. (1992). The 1991 Sierra Madre earthquake sequence in southern California: seismological and tectonic analysis, *J. Geophys. Res.* (submitted for publication).

Hauksson, E. and L. M. Jones (1991). The 1988 and 1990 Upland earthquakes: left-lateral faulting adjacent to the central Transverse Ranges, *J. Geophys. Res.* **96**, 8143–8165.

Houston, H (1990a). Broadband source spectra, seismic energy, and stress drop of the 1989 Macquarie Ridge earthquake, *Geophys. Res. Lett.* **17**, 1021–1024.

Houston, H (1990b). A comparison of broadband source spectra, seismic energies, and stress drops of the 1989 Loma Prieta and 1988 Armenian earthquakes, *Geophys. Res. Lett.* **17**, 1413–1416.

Hutton, L. K. and D. M. Boore (1987). The M_L scale in southern California, *Bull. Seism. Soc. Am.* **77**, 2074–2094.

Jennings, P. C. and H. Kanamori (1983). Effect of distance on local magnitudes found from strong-motion records, *Bull. Seism. Soc. Am.* **73**, 265–280.

Jones, L. M., K. E. Sieh, E. Hauksson, and L. K. Hutton (1990). The 3 December 1988 Pasadena, California earthquake: evidence for strike-slip motion on the Raymond fault, *Bull. Seism. Soc. Am.* **80**, 474–482.

Joyner, W. B. and D. M. Boore (1981). Peak horizontal acceleration and velocity from strong-motion records, including records from the 1979 Imperial Valley, California, earthquake, *Bull. Seism. Soc. Am.* **71**, 2011–2038.

Kanamori, H. (1977). The energy release in great earthquakes, *J. Geophys. Res.* **82**, 2981–2987.

Kanamori, H. (1990). *Pasadena very-broad-band system and its use for real-time seismology, extended abstract for the U.S.-Japan Seminar on Earthquake Prediction, Morro Bay, California, 12–15 September, 1988, U. S. Geol. Surv. Open-File Rept. 90-98*,

Kanamori, H. and C. R. Allen (1986). Earthquake repeat time and average stress drop, in *Earthquake Source Mechanics*, S. Das and C. H. Scholz (Editors), American Geophysical Union, Washington D.C., 227–235.

Kanamori, H., E. Hauksson, and T. Heaton (1991). TERRAscope and CUBE project at Caltech, *Eos* **72**, 564.

Kanamori, H., J. Mori, and T. H. Heaton (1990). The 3 December 1988, Pasadena earthquake (M_L = 4.9) recorded with the very broadband system in Pasadena, *Bull. Seism. Soc. Am.* **80**, 483–487.

Kanamori, H., H.-K. Thio, D. Dreger, E. Hauksson, and T. Heaton (1992). Initial investigation of the Landers, California, earthquake of 28 June 1992 Using TERRAscope, *Geophys. Res. Lett.* **19**, 2267–2270.

Kikuchi, M. and Y. Fukao (1988). Seismic wave energy inferred from long-period body wave inversion, *Bull. Seism. Soc. Am.* **78**, 1707–1724.

Mori, J. and S. Hartzell (1990). Source inversion of the 1988 Upland, California, earthquake: determination of a fault plane for a small event, *Bull. Seism. Soc. Am.* **80**, 507–518.

Orowan, E. (1960). Mechanism of seismic faulting, *Geol. Soc. Am. Mem.* **79**, 323–345.

Richter, C. (1935). An instrumental earthquake magnitude scale, *Bull. Seism. Soc. Am.* **25**, 1–32.

Somerville, P. G., J. P. McLaren, L. V. LeFevre, R. W. Burger, and D. V. Helmberger (1987). Comparison of source scaling relations of eastern and western North American earthquakes, *Bull. Seism. Soc. Am.* **77**, 322–346.

Thatcher, W. and T. C. Hanks (1973). Source parameters of southern California earthquakes, *J. Geophys. Res.* **78**, 8547–8576.

Uhrhammer, R. A. and E. R. Collins (1990). Synthesis of Wood-Anderson seismograms from broadband digital records, *Bull. Seism. Soc. Am.* **80**, 702–716.

Vassiliou, M. S. and H. Kanamori (1982). The energy release in earthquakes, *Bull. Seism. Soc. Am.* **72**, 371–387.

SEISMOLOGICAL LABORATORY
CALIFORNIA INSTITUTE OF TECHNOLOGY
PASADENA, CALIFORNIA 91125
(H.K., E.H., L.K.H.)

U.S. GEOLOGICAL SURVEY
PASADENA, CALIFORNIA 91106
(J.M., T.H.H., L.M.J.)

Manuscript received 22 June 1992